Optical Engineering

SPIEDigitalLibrary.org/oe

Segmented vortex telescope and its tolerance to diffraction effects and primary aberrations

Juan P. Treviño
Omar López-Cruz
Sabino Chávez-Cerda

Segmented vortex telescope and its tolerance to diffraction effects and primary aberrations

Juan P. Treviño
Omar López-Cruz
Sabino Chávez-Cerda
Instituto Nacional de Astrofísica
Optica y Electrónica
Apartado Postal 51/216
Puebla, México 72000
E-mail: trevinojp@inaoep.mx,
trevino.juanpablo@gmail.com

Abstract. The segmented large millimeter telescope (LMT/GTM) is the largest spatial light modulator capable of producing vortex beams of integer topological charge. This observing mode could be applied for direct exoplanet searches in the millimeter or submillimeter regimes. The stability of the vortex structure against aberrations and diffraction effects inherent to the size and segmented nature of the collector mirror was studied. In the presence of low-order aberrations, the focal distribution of the system remains stable. Results show that these effects depend on the topological charge of the vortex and the relative orientation of the aberration with respect to the antenna axis. Coma and defocus show no large effects in the image at the focal plane; however, the system is very sensitive to astigmatism. Heat turbulence, simulated by random aberrations, shows that the system behaves in a similar way as astigmatism dissociating the vortices. The segmented vortex telescope is proposed as a novel approach for the detection of giant planets outside circumstellar disks around nearby stars. Since results are applicable to other facilities with segmented surfaces, it is suggested that this idea should be considered as a regular observation mode complementary to interferometric methods.
 [DOI: 10.1117/1.OE.52.8.081605]

Subject terms: aberrations; astronomy; diffraction; millimeter waves; phase modulators; planets; spatial light modulators; telescopes.

Paper 121455SS received Oct. 4, 2012; revised manuscript received Jan. 23, 2013; accepted for publication Jan. 24, 2013; published online Feb. 21, 2013; corrected Mar. 6, 2013.

1 Introduction

In general, waves with phase singularities and a rotational flow around the singularity are called vortices. Vortex fields arise in nature[1] and enjoy a large number of technological applications. Vortex fields are found in physical systems covering the widest range of scales, from single photons to astronomical black holes.[2] Applications of vortex fields have been found in optics, acoustics, telecommunications, astronomy, and other fields.[3]

In astronomy, light vorticity has attracted a lot of attention since it has shown to be an elegant and efficient way to reject light from a bright source on axis, allowing the study of its surroundings. Remarkable results have been obtained by the direct imaging of exoplanetary systems using ground-base optical telescopes equipped with coronagraphs.[4–9]

Vortex fields have been recently introduced to increase the number of independent channels available to transmit data signals. By reshaping a common parabolic antenna, a phase vortex can be induced on a transmitted wave, creating a set of channels which are independent to those of a regular antenna.[10,11] The number of channels that can be transmitted using a single frequency is, in principle, unbounded. This application has the potential of revolutionizing telecommunications.

In this work, by combining the ideas above, we explore the feasibility of turning the large millimeter telescope (LMT/GTM)[12] into a coronagraph at millimeter wavelengths by reshaping its segmented collector mirror into a vortex generator. The main purpose is to investigate the potential of this system as a regular observational mode able to detect giant exoplanets or giant proto-exoplanets outside circumstellar disks. Given the lower luminosity contrast of such objects in millimeter wavelengths, this device would be very suitable for this application. We have investigated the stability of the system against diffraction effects induced by the segmented nature of the primary surface and possible damage to its segments. We took into account the effects of aberrations inherent to such large structure, as those produced by deformations on the primary mirror due to its own weight or by temperature variations on its 50 m diameter surface and its surroundings.[13]

2 Optical Vortices and Phase Modifying Devices

A vortex coronagraph is created by placing a phase modifying device at the focal plane of an optical system.[4,6–9] At a relayed pupil plane most of the radiation from on-axis sources is concentrated in a sharp ring that can be easily filtered away by means of a stop known as Lyot stop. This setup is useful because it allows to filter out light from on-axis sources. Radiation from off-axis sources remains almost unchanged when it goes through the system. In this way it is possible to explore the vicinity of very bright objects and even to produce images of objects dimmer and angularly close to the primary one.

For telescopes at millimeter wavelengths, any component intended to be implemented at the focal plane poses a technical challenge, since any element at this plane will attenuate the already low-intensity signals. Additionally, detection devices need to be kept at low temperatures to maximize their sensitivity,[14] so any additional element absorbs some

0091-3286/2013/$25.00 © 2013 SPIE

of the incident radiation and requires cooling which implies a higher cost of the entire system. Therefore, a vortex phase mask at the focal plane would not be the best option for radio and millimeter signals, hence we explore the possibility to locate the vortex on the primary surface.

The LMT/GTM has a Cassegrain design that operates at millimeter wavelengths.[12] Our proposal is to reshape the segmented primary surface to produce vortices at the working wavelengths of this telescope, which are 1.1, 1.4, and 2.1 mm.[15,16] The independent control of the segments in the primary mirror can be configured to produce integral order vortices at such wavelengths.

Generating a vortex at the exit pupil creates a doughnut-like field distribution at the focal plane. Such setup is the reverse of the signal transmission implemented in Refs. 10 and 11. The detection device currently used at the LMT/GTM is a bolometer array composed of 144 pixels.[15] The beam size is reduced before it reaches the bolometer array. This way if the vortex distribution had a larger radius than the bolometer array, a further beam reduction would be necessary; however, this adjustment is straightforward. This configuration was first explored as a means to reject light form bright sources by opening a window to observe incoherent background. In principle, the achievable contrast depends on the vortex order and the size of a field stop located at the focal plane. For two incoherent sources, the achievable contrast could be of the order of 10^5, so it is possible to detect Super-Jupiters. Although not common in nature, for a pair of coherent sources, both on-axis and off-axis sources will come across the same vortex. However, some basic rules can be given for the detection of secondary sources.[5]

3 Vortex Collector Mirror

An optical vortex is a wavefield with an azimuthally varying phase factor of the form $e^{im\varphi}$. The number $m \neq 0$ must take only integral values and is known as the topological charge of the vortex. The argument $m\varphi$ in the exponential represents an azimuthal linear variation of the phase which generates a helical wavefront. The corresponding Poynting vector field follows helical trajectories as well. These kind of wavefields are known to carry orbital angular momentum.[3,17] As a consequence, part of the radiation in the center of the beam is driven away from the propagation axis and a dark core is created at its center.

A Cassegrain telescope like the LMT/GTM is described by a complex pupil function whose mathematical representation includes information about the optical power and aberrations of the system. If the vortex is introduced at the exit pupil of the telescope, the mathematical expression of the field in this plane is

$$U_0(r,\varphi) = T_0(r,\varphi)\exp\left[-ik\left(\frac{r^2}{2f}\right)\right]e^{ikW(r,\varphi)}e^{im\varphi}, \tag{1}$$

where $W(r,\varphi)$ is the aberration function and f is the focal distance of the mirror. The wavenumber is given by $k = 2\pi/\lambda$ for the wavelength λ, while m is an integer defining the topological charge of the vortex.

The comparative sizes between the working wavelengths and the gaps of the LMT/GTM are such that diffraction effects can be neglected. However, diffraction effects caused by gaps between segments have been investigated here including different gap sizes and configurations.

The field U at planes approaching the neighborhood of the focal plane $z = f^-$ is obtained by a Fresnel diffraction integral, while at the focal plane $z = f$ the integral transforms into the Frounhofer diffraction integral given by

$$U_f(\rho,\theta) = \mathcal{C}\int_{-\pi}^{\pi}\int_0^{\infty} T_0(r,\varphi)e^{ikW(r,\varphi)}e^{im\varphi} \times \exp\left[i\frac{2\pi}{\lambda f}r\rho\cos(\varphi-\theta)\right]r\mathrm{d}r\mathrm{d}\varphi, \tag{2}$$

where $\mathcal{C}$ is a complex constant related to the amplitude of the field. For a continuous mirror and in the total absence of aberrations, the field at the focal plane is radially symmetric and it reduces to the Hankel transform of order m of the transmission function $T_0(r)$. In the general case that we will study here a two-dimensional Fourier transfrom will be necessary as the circular symmetry of T_0 may be broken by arbitrary aberrations or diffraction effects due to large gaps and damaged panels. For nonsymmetric cases, we evaluate numerically Eq. (2) by means of a fast Fourier transform algorithm. In order to calibrate our numerical simulation we evaluated first the $m = 0$ case and other cases for which analytical solutions are available, with known parameters. For other values of m we also checked the phase of the focal field for consistency.

4 Reshaping the LMT/GTM Primary Surface

In the original design the collector mirror of the LMT/GTM has a 50 m diameter and a radius of curvature of 35 m. It is composed of 180 panels arranged in five rings. The innermost ring is formed of 12 segments, the second ring has 24, and the remaining three are composed of 48 panels. The length of each panel is 5 m and the corresponding angular extent depends on the ring where the segment is located. Currently, only the first three inner rings are operational, the corresponding diameter is of 32 m. It is feasible to implement our study to the current size of the primary, hence we have adjusted our simulations to the current diameter (see Fig. 1). Considering the full 50 m aperture is straightforward.

Currently, each segment of the primary mirror in the LMT/GTM is controlled by three actuators with a maximum displacement of 5200 μm. The total wavefront error of the LMT/GTM design is of 75 μm rms which means $\epsilon < \lambda/20$ at 1.5 mm. The collector alone should have a 55 μm rms error which represents $\epsilon \approx \lambda/18$ at 1 mm. For longer wavelengths the error decreases. The secondary mirror is a hyperbolic surface with a diameter of 2570 mm which represents a central obscuration of less than 10% the radius of the exit pupil. The secondary has six degrees of freedom.

To create a vortex of order m at the collector mirror, the reflected converging wave must have an additional azimuthal phase $m\varphi$. For this reason, the collector must have a linear azimuthal deformation with a maximum of $m\lambda/2$ additional to its parabolic profile. For every ring, each one of the N junctions between sectors should be displaced by $\frac{m\lambda}{2}\frac{n}{N}$, where $n = 0, 1, \ldots N$, and N is the number of segments in the corresponding ring. The maximum possible displacement of the segments allows for the creation of an $m = 5$ vortex at $\lambda = 2$ mm. However, if the desired vortex order and corresponding wavelength required a maximum

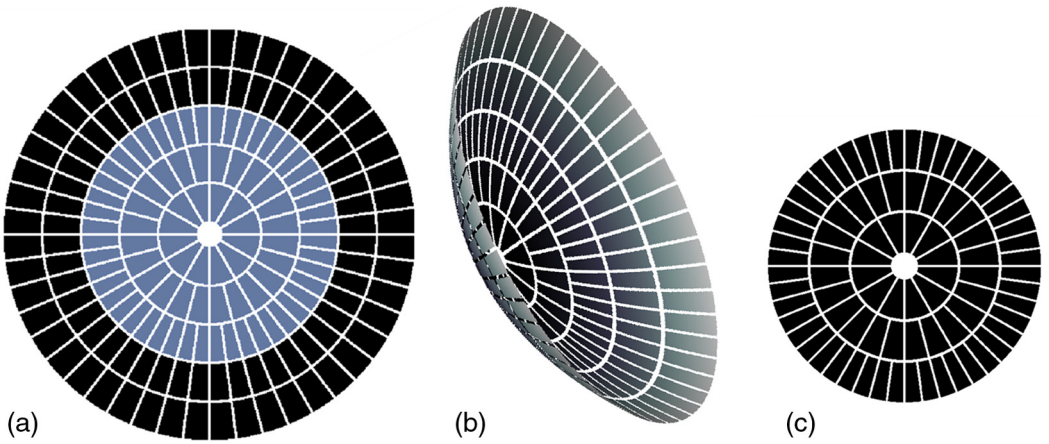

Fig. 1 (a) Complete setup with five rings as originally designed. Segments in black are currently not active. (b) The collector mirror of the LMT/GTM generates a waveftont with this shape. The lines correspond to the gaps between the telescope segments. (c) Front view of the transmittance function of the current three rings of the collector.

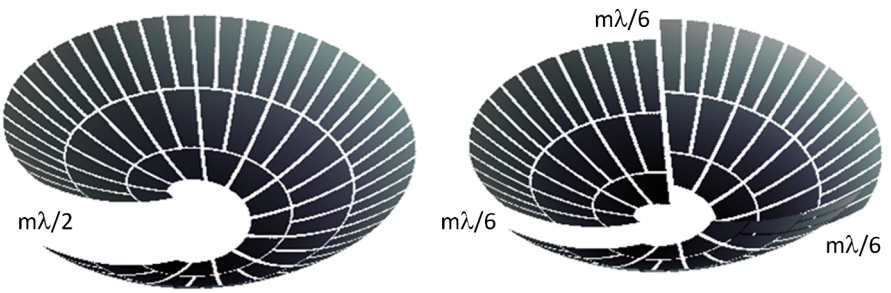

Fig. 2 Multiple pitch mirror for the segmented vortex telescope (SVT).

displacement larger than the maximum possible for a single segment, there is an option of creating a multiple pitch vortex, as shown in Fig. 2. This configuration gives the same reflected wavefront but the physical displacements required are smaller.

It is worth mentioning that these calculations are independent of the number of segments in the collector mirror because the surface produced has a ramp-like profile in the azimuthal direction, which in turn produces a true spiral wavefront. Deforming the primary surface of the LMT/GTM as proposed here does not induce aberrations, it reshapes the wavefront into a convergent helicoid affected by diffraction due to segment gaps. The rigidity of the collector mirror segments might cause errors when achieving the value of m; however the surface accuracy is below the error the system tolerates (approximately 5%) and they can be neglected. This procedure to produce vortices might be compared to a step spiral phase mask[18] with N steps. The latter approximates the ideal spiral wavefront by superposing N plane waves with a relative retardation. This approximation causes a dependence on N for such device, as opposed to the deformation of the primary segmented mirror studied here.

5 Stability Analysis to Diffractive Perturbations

As mentioned before, in the LMT/GTM the gaps are sufficiently small compared to the wavelengths at which the system operates; nevertheless we present simulations to evaluate the diffraction effects that would appear for larger gaps. We split the problem to study radial and angular gaps separately.

We first evaluate pupils formed from several continuous rings having a variable separation. The transmittance function of such a pupil is represented as a sum of circ functions. Given the linearity of the Fourier transform, the focal field of this multiple ring pupil is a sum of the corresponding Fourier transforms. For any value of m, the effect on the focal distribution is very similar to what happens with a simple annular pupil: the focal distribution shrinks radially, and the main maximum decreases relative to the secondary maximum as the radius of central obscuration increases (Fig. 3). This effect is interpreted as having an increase of resolution of the system but a contrast decrease. For different values of m the maximum field amplitude values drop almost linearly as the size gap increases. Nevertheless, the profile appears to be a scaled version of the original one; therefore the resulting distribution can be always approximated by a power law r^m in the vicinity of the vortex core.

Next we will consider the case in which a complete sector of angle φ is lost or darkened. For topological charges $m > 1$ an obscured sector causes the vortex to dissociate and generate m dark regions in the focal image. The topological charge of a vortex must be preserved along propagation; therefore these dark regions are associated to individual vortices with unitary charge. In general, vortices with opposite charge might cancel each other upon propagation while vortices with the same charge might travel alongside each other for long distances. Detailed information on vortex propagation might be found in Refs. 19 and 20. In the case presented here vortex dissociation happens as the m-order phase singularity separates into m first-order singularities as shown

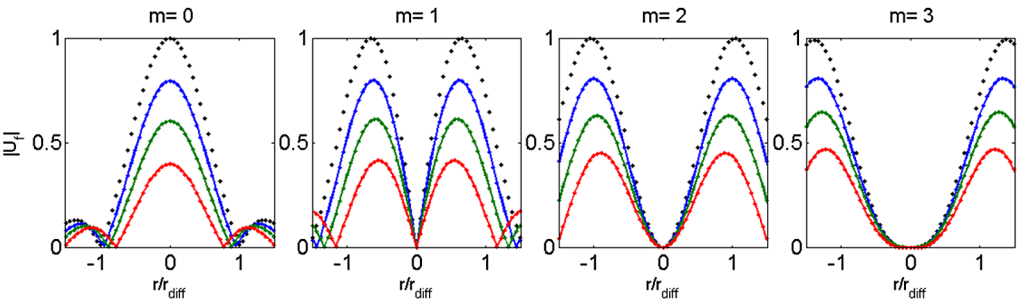

Fig. 3 Transverse section of the normalized field amplitude at the focal plane for a pupil with three rings. The different lines show how the intensity drops as the gap between rings increases. The maximum amplitude as a function of the gap size ratio decreases almost linearly.

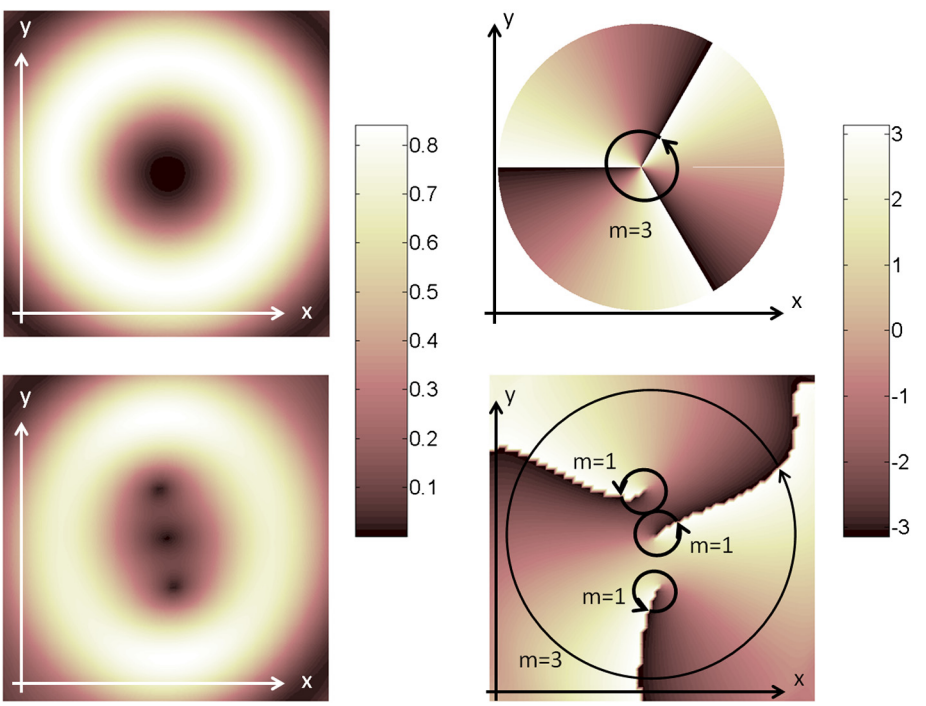

Fig. 4 Phase and normalized amplitude at the focal plane for an $m = 3$ vortex (top) dissociated into three $m = 1$ vortices (bottom).

in Fig. 4. A similar effect happens when the system is illuminated by two separate coherent sources.[5] However, the relative position of the dark regions due to the existence of multiple sources and that due to aberrations behave differently.

Vortex dissociation is clearly appreciated if we observe the phase of the field, but it could be difficult to see with intensity detectors because the phase information is lost and vortices manifest as local minima. However we might define a criterion to determine vortex dissociation depending on the contrast resolution of the detection device.

The vortex dissociation effect is also observed for damaged segments as small as $\varphi \sim 10$ deg which is a very small value for the angular extent of the real LMT/GTM segments. In this case the vortex structure is unstable because symmetry is broken (Fig. 5). The focal distribution can be recovered to some extent if the opposite segment is darkened since some symmetry is recovered. We can see in the figure that for $m = 4$ the original profile is recovered in the vertical section. The case for $m = 2$ is not fully recovered; however the horizontal section remains with the same profile but a lower contrast.

Next, we examine when many opposite sectors are lost or obscured as shown in Fig. 6. A transverse section of the amplitude at the focal plane shows that although the maximum decreases, the profile of the central dark area caused by the vortex remains unchanged. The same effects happen for the second or third rings composed of more segments. In these outer rings there is a larger number of segments that contribute to the focal field, and although the obscured proportion might be high, the opposite reflecting sectors reconstruct a more symmetrical pattern.

If the missing panels are considered to be radial as shown (Fig. 6), the maximum field amplitude decreases linearly for $m = 0$, but for larger values of m, the behavior departs slightly from linearity. In all cases the drop is proportional to the nonreflecting area.

We have analyzed diffraction effect due to gaps size and found out that the central annular field is stable up to a ten to one ratio between the panel and the gap. In the LMT/GTM the real proportion is much smaller than the aforementioned ratio. For this reason, the effect can be neglected.

We now consider the effects of damaged panels. We model this situation by leaving out randomly selecting panels

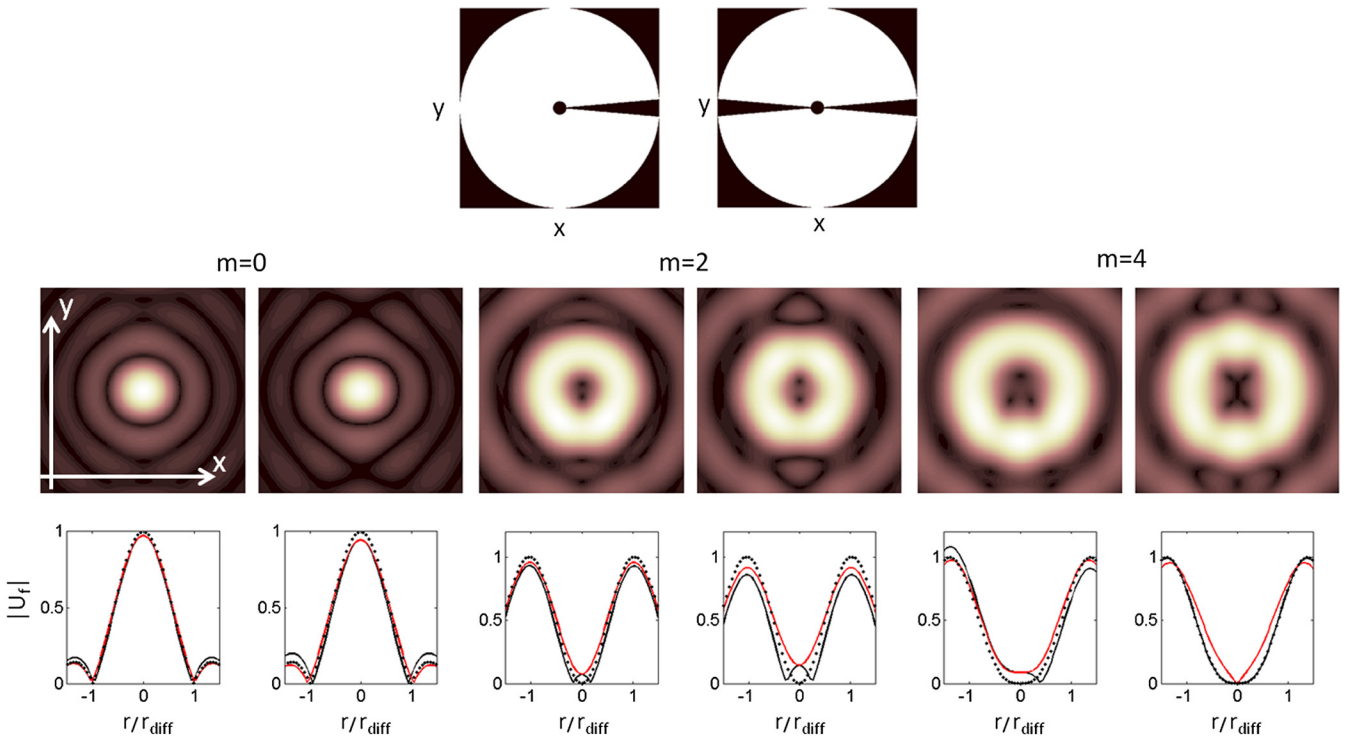

Fig. 5 A complete damaged sector breaks the symmetry of the system and causes vortex dissociation for small damaged angles. The top images represent the obscured sectors. Second and third rows show the normalized field amplitude distribution and a cross-section, respectively, for $m = 0$, $m = 2$, and $m = 4$ (bottom) imaged with a damaged sector of $\phi = 15$ deg. The dotted line is the normalized amplitude with a nondamaged pupil, while the solid lines are vertical (black) and horizontal (red) cross-sections of the amplitude with damaged pupils. Notice the dips that correspond to the dissociated vortices.

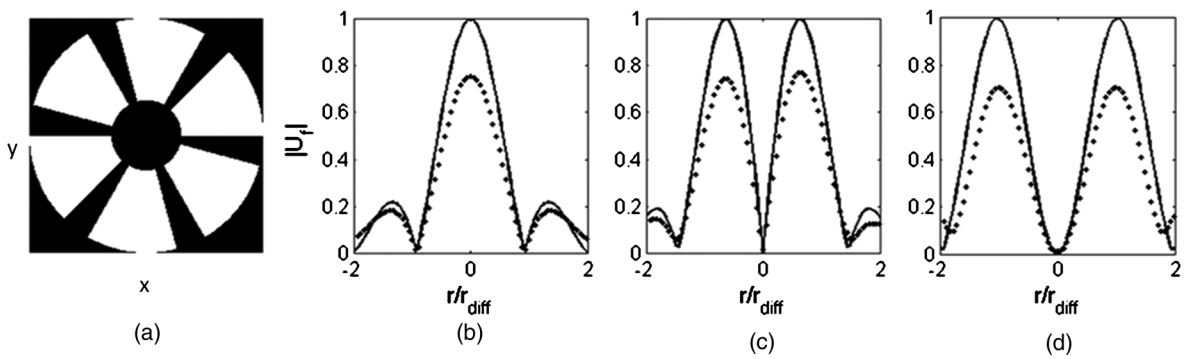

Fig. 6 (a) Segmented ring pupil with gap ratio of 1/4. (b) $m = 0$, (c) $m = 1$, and (d) $m = 3$. The solid line is the normalized field amplitude for a continuous ring, while the dotted line is for the segmented one. The intensity field drops as the gap size ratio increases, but the shape of the field is preserved.

(Fig. 7). We observe again that the basic vortex structure due to the azimuthal phase is maintained. Similar situations involving partially obstructed optical vortices have shown that this type of fields are stable upon propagation.[21] Even the absence of a complete ring, which is a special case of concentric ring pupil, was considered. It can be seen that this can have small effects on the expected image (Fig. 7).

6 Stability Analysis under Aberrations

So far we have analyzed how robust the segmented vortex telescope (SVT) can be considering diffraction perturbations due to gaps between panels or assuming damages of the collector surface. We now draw the attention to the presence of aberrations, e.g., Seidel or balanced aberrations.[22,23] Typically, the atmospheric turbulence is modeled by a distribution of aberrations. For the LMT/GTM, in addition to atmospheric turbulence, gravitational effects cause deformations of the collector mirror and also temperature fluctuations across its 50-m diameter surface cause aberrations.[13] For this reason, we analyze the focal distribution of the vortex telescope given Seidel and balanced aberrations and also random phase aberrations.

We introduce the wave aberration of the system as a factor $e^{ikW(r,\varphi)}$, with $W(r,\varphi) = A_j\Phi_j(r,\varphi)$ and Φ_j could be either a Seidel or a balanced (Zernike) aberration.[22,23] The aberration coefficient A_n is given in units of the wavelength λ. We used Seidel spherical aberration, Seidel and Zernike astigmatism, and finally Seidel and Zernike coma.

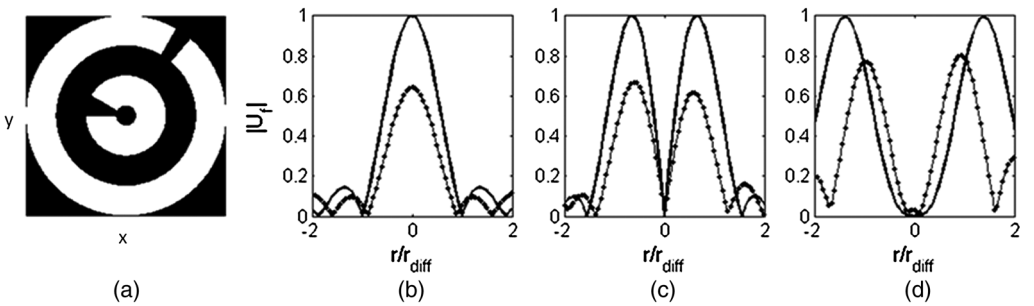

Fig. 7 (a) A pupil with full ring and random segments damaged. (b) $m = 0$, (c) $m = 1$, and (d) $m = 3$. The solid line is the field intensity for a continuous ring, while the dotted line is for the damaged one. The intensity field drops but the shape of the field is preserved.

Different aberration coefficients were selected to evaluate the stability of the central vortex structure at the focal plane as in the previous cases. The aberration coefficients were chosen according to acceptable Strehl ratio criteria[24] selecting coefficients $A_i \leq 0.30$. Symmetric aberrations such as defocus or first- and second-order spheres cause variations in the contrast of the focal image. Nevertheless the central profile of dark regions remains the same in the sense that a power law fit in the radial variable is still possible in the vicinity of the vortex core. If the symmetry is broken by aberrations, the vortex dissociates in a similar way as with perturbations due to diffraction. Astigmatic aberration given by $W = r^2 \cos\phi$ generated visible vortex dissociation for low values, $A_a = 0.03$. Nevertheless, the proportion of the inner maxima to the main ring was about 5%. We set this proportion here to define a visible dissociated vortex. Vortex dissociation occurs in an angle $\pi/4$ from the astigmatism axis, and a section perpendicular to this keeps the r^m power law profile. The simulations shown in Fig. 8 include transversal sections of the focal distribution of amplitude to show how the zeros are separated depending on the value of A_a. For larger values of astigmatism the radiation distribution is deformed into a set of intensity lobes related to Hermite-Gaussian modes. It is known that Hermite-Gaussian modes can be converted to and from Laguerre-Gaussian (L-G) modes by means of an astigmatic mode converters. The latter are a type of vortex wavefields.[25] The system's response to aberration of coma ($W = r^3 \cos\phi$) was more stable since no vortex dissociation was observed for aberration coefficients $A_c < 0.35$ while the critical value for a 0.8 Strehl ratio is $A_c = 0.21$.

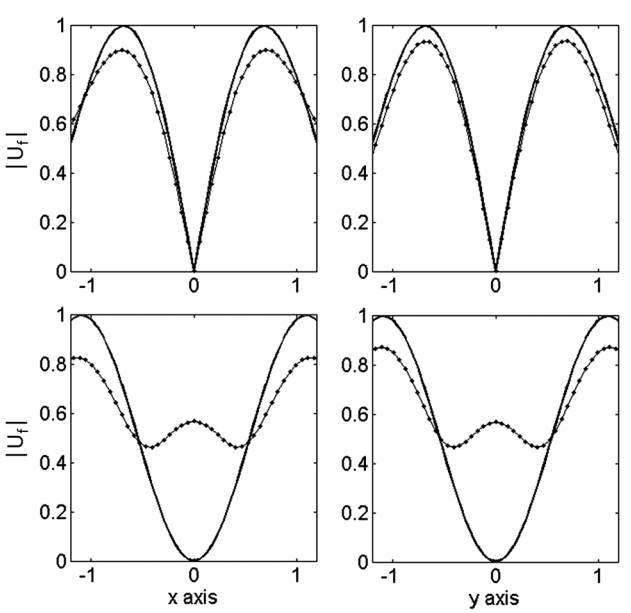

Fig. 8 Cross-sections of intensity at the focal plane for pupil with astigmatic aberration $A_a = 0.3$ (dashed lines) and the unaberrated reference (solid line). Top: $m = 1$, Bottom: $m = 2$.

A system with randomly damaged panels and a Seidel aberration combined shows that the effects observed are closer to those produced by aberration alone. The dark region at the focal plane dissociates for aberration coefficients similar to those without segment loss. Figure 9 shows the collector mirror with obscured panels and $A_c = 0.15$ along with the focal image and transverse section. The image shows vortex dissociation and small diffraction effects.

For the large area of the collector mirror it is expected that inhomogeneities of air density caused by atmospheric fluctuations or heat turbulence will generate a high-order random aberration of the incoming wavefront. The thermal design of the LMT/GTM allows to evaluate and compensate deformations of the primary due to heat turbulence.[13] However, the small fluctuations might not be possible to compensate. In order to investigate the influence of this type of perturbation on the system, we produced a surface with random distributions of various frequencies (Fig. 10). Each case was modeled for Seidel aberrations and the aberration-free case. In each case we found out vortex dissociation for a phase aberration of a quarter wavelength measured peak to peak (Fig. 11). The sensitivity of the system to this type of aberration requires a careful calibration and wavefront compensation of the system.

Since the antenna follows objects in the sky, astigmatism caused by deformation of the collector mirror due to gravity is constantly changing. If we wanted to distinguish between the presence of aberrations and double coherent sources, we might have to analyze the behavior of the dark regions as the antenna scans a given object in the sky. Aberrations caused by changes in the antenna position would cause the dark regions to move as the antenna moves. On the other hand, if the dark regions remain unchanged as the scanning goes on, it would mean that there is a double source. More precise schemes are being investigated by our group at the moment, and a report will be developed.

7 Astronomical Application

Consider the LMT/GTM working at 1.1 mm; at this wavelength the field of view is 1.5′ (minutes of arc) and a beam size of 5″ (seconds of arc) with a pointing accuracy is 1″. The specified final surface accuracy is 70 μm; this results in an antenna efficiency of 46% at this wavelength. In the

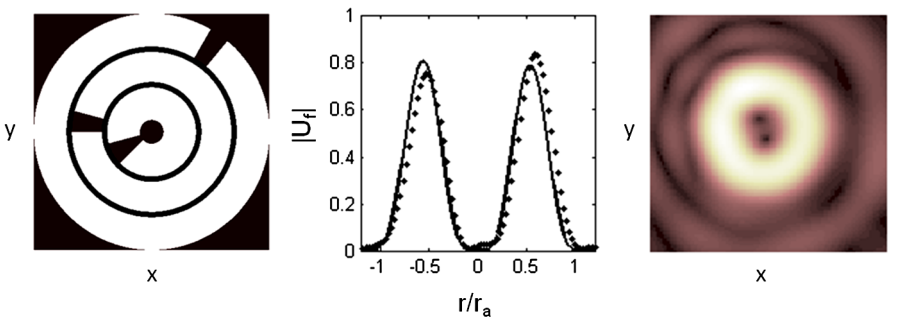

Fig. 9 A case combining damaged random segments and aberration of coma. The solid line represents the ideal case.

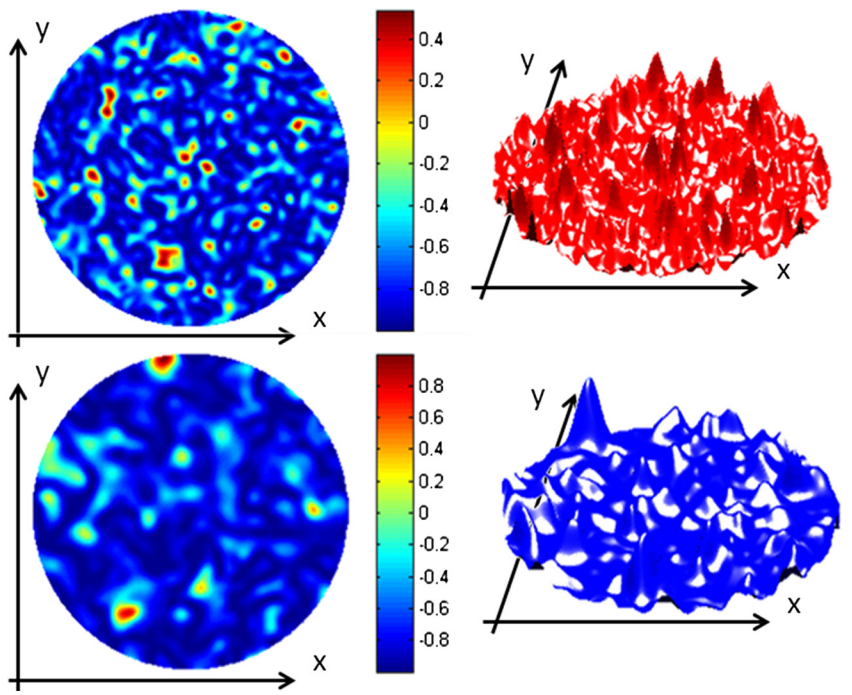

Fig. 10 Wavefront aberration surface generated from a random frequency distribution. Top: high frequencies. Bottom: low frequencies.

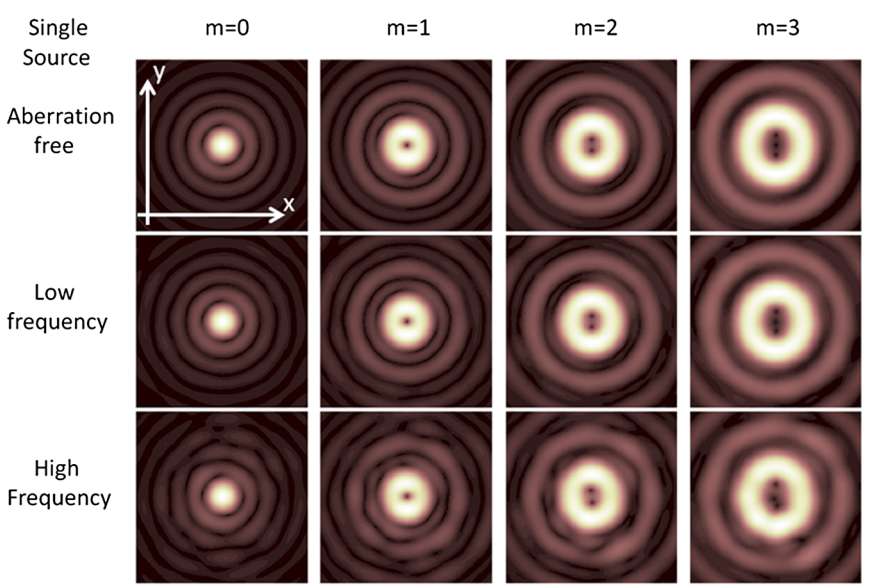

Fig. 11 Fluctuations generating a random phase aberration of a quarter wavelength peak to peak dissociates vortices.

millimeter regime the contrast between the luminosity of a solar-like host star ($T_{\text{eff}} \sim 6000$ K) and a Super-Jupiter ($T_{S-J} \sim 1700$ K, $R_{S-\text{Jupiter}} \sim 1.5 R_{\text{Jupiter}}$[26]) becomes of the order of 10^3, while in the optical regime the contrast could be several times higher up to $\sim 10^8$. However, cold dust in circumstellar disks becomes the dominant source of radiation at 1 mm, hence the contrast between a face-on circumstellar disk (mean $T_{\text{Disk}} \sim 50$ K, see below for average size)[27] and a Super-Jupiter could be as large as 10^{-6}. These are rough figures under the assumption that the host star, the circumstellar disk, and the planet emit as black bodies.

The mode of the diameter distribution of circumstellar disks[28] is about 300 AU (1 astronomical unit = 149,597,870.691 km). A disks of about this size would appear unresolved at 60 pc (1 parsec = 206265 AU); hence we can use LMT/GTM in the SVT mode as a coronagraph to search for exoplanets orbiting around star-circumstellar disks systems at distances larger than 60 pc. The LMT/GTM's field of view would cover separations larger than 5000 AU from the host star. Guided by previous observations,[29] we found that exoplanetary systems have shown a wide variety of configurations. Massive planets have been found to orbit their host stars at wide orbits, ranging from several hundreds to over a thousand AU, from their host stars.[30] A comprehensive survey for massive planets at wide orbits could help to impose constraints on the origin of exoplanets and their relation with the environment.[31] Super-Jupiter have properties similar to a low-mass brown dwarf, hence LTM/GTM working as SVT could also help to study the frequency of brown dwarfs in multistellar systems.

The geometry of circumstellar disks can be explored using sub-Rayleigh resolution[32] in classically resolved, or unresolved circumstellar disks, or in the case of stellar systems with multiple components (stars and planets), this mode can increase the resolution up to $0.5''$ at 1.1 mm, which can only be attained with interferometric arrays. Moreover, the high mapping speeds ($0.55\ \text{deg}^2/\text{hr}/\text{mJy}^2$ for LMT/GTM with AzTEC) of large single dish telescopes make them more efficient than interferometric arrays. Therefore, we suggest that future large millimeter single dish telescope should consider SVT as a regular observational mode, which would guide follow-up observations with interferometric arrays.

8 Conclusions

We have investigated the properties of the large millimeter telescope as the largest spatial electromagnetic wavefront light modulator capable of producing vortex beams of integer topological charge at selected wavelengths. We studied its stability against diffraction and aberration perturbations.

Diffraction caused by gaps between segments and by possible mechanical damages of the LMT/GTM panels is not critical since the main features of the vortex structure at the focal plane remain unaffected by the segmented nature of the telescope even in highly perturbed cases.

Regarding aberrations, for small values of defocus and coma, the focal distribution of the system remains stable. As expected, we observed that the system is very sensitive to astigmatism. Nonradially symmetric aberrations cause the vortex to dissociate into m vortices, and as a result, dark zones appear in the focal distribution. The values at which this happens depend on m and on the relative orientation of the aberrations. The dark zones of a single source always appear perpendicular to the aberration axis.

For aberrations with random wavefront distribution, simulating heat turbulence, the system shows a high sensitivity which must be taken into account since even single sources produce vortex dissociation generating similar focal distributions as those produced by two coherent sources. In general, single sources produce multiple dark regions at the focal plane when the symmetry of the system is broken either by diffraction or by the presence of nonsymmetric aberrations.

The LMT/GTM working as an SVT could offer unprecedented opportunities for exoplanetary studies. The SVT can help to search for giant planets (Super-Jupiters) outside debris disks[33] and also work in the sub-Rayleigh[32] mode to resolve multiple components.

Acknowledgments

The authors would like to acknowledge the reviewers of this manuscripts. Their valuable comments helped us to improve significantly our work. They also wish to dedicate this work to Alfonso Serrano Perez-Grovas. The first author would like to acknowledge Alfredo Agustin Montaña Barbano for the valuable sources for the development of this work. He would also like to acknowledge Jesus Emmanuel Gomez-Correa for fruitful discussion.

References

1. M. Berry, "Making waves in physics. Three wave singularities from the miraculous 1830s," *Nature* **403**(6765), 21 (2000).
2. F. Tamburini et al., "Twisting of light around rotating black holes," *Nat. Phys.* **7**(3), 195–197 (2011).
3. A. M. Yao and M. J. Padgett, "Orbital angular momentum: origins, behavior and applications," *Adv. Opt. Photon.* **3**(2), 161–204 (2011).
4. A. G. Swartzlander, Jr. et al., "Astronomical demonstration of anoptical vortex coronagraph," *Opt. Express* **16**(14), 10200–10207 (2008).
5. G. A. Swartzlander, Jr., "Peering into darkness with a vortex spatial filter," *Opt. Lett.* **26**(8), 497–499 (2001).
6. G. Foo, D. M. Palacios, and A. G. Swartzlander Jr., "Optical vortex coronagraph," *Opt. Lett.* **30**(24), 3308–3310 (2005).
7. D. Mawet et al., "Annular groove phase mask coronagraph," *Astrophys. J.* **633**(2), 1191–1200 (2005).
8. E. Serabyn, D. Mawet, and R. Burruss, "An image of an exoplanet separated by two diffraction beamwidths from a star," *Nature* **464**(7291), 1018–1020 (2010).
9. G. J. Ruane and G. A. Swartzlander, "Optical vortex coronagraphy with an elliptical aperture," *Appl. Opt.* **52**(2), 171–176 (2013).
10. F. Tamburini et al., "Encoding many channels on the same frequency through radio vorticity: first experimental test," *New J. Phys.* **14**(3), 033001 (2012).
11. B. Thidé et al., "Radio beam vortiity and orbital angular momentum," *Instrum. Methods Astrophys.* arXiv:1101.6015v1 [astro-ph.IM] (2011).
12. W. M. Irvine, E. Carrasco, and I. Aretxaga, *The Large Millimeter Telescope: Neighbors Explore the Cosmos*, INAOE, Pue, Mexico (2005).
13. H. J. Kaercher and J. W. M. Baars, "Design of the large millimeter telescope/gran telescopio millimetrico (LMT/GTM)," *Proc. SPIE* **4015**, 155–168 (2000).
14. J. Glenn et.al., "Bolocam: a millimeter-wave bolometric camera," *Proc. SPIE* **3357**, 326–334 (1998).
15. G. W. Wilson et al., "The aztec mm wavelength camera," *Mon. Not. R. Astron. Soc.* **386**(2), 807–818 (2008).
16. G. W. Wilson et al., "Aztec millimetre survey of the cosmos field—I. Data reduction and source catalogue," *Mon. Not. R. Astron. Soc.* **385**(4), 2225–2238 (2008).
17. L. Allen et al., "Orbital angular momentum of light and the transformation of Laguerre-Gaussian laser modes," *Phys. Rev. A* **45**(11), 8185–8189 (1992).
18. E. Mari et al., "Fabrication and testing of 1 = 2 optical vortex phase masks for coronography," *Opt. Express* **18**(3), 2339–2344 (2010).
19. S. Chávez-Cerda, J. C. Gutiérrez-Vega, and G. H. C. New, "Elliptic vortices of electromagnetic wave fields," *Opt. Lett.* **26**(22), 1803–1805 (2001).
20. G. Indebetow, "Optical vortices and their propagation," *J. Mod. Opt.* **40**(1), 73–87 (1993).

21. R. Rop, I. A. Litvin, and A. Forbes, "Generation and propagation dynamics of obstructed and unobstructed rotating orbital angular momentum-carrying helicon beams," *J. Opt.* **14**(3), 035702 (2012).
22. V. N. Mahajan, "Zernike circle polynomials and optical aberrations of systems with circular pupils," *Appl. Opt.* **33**(34), 8121 (1994).
23. V. N. Mahajan, "Zernike annular polynomials and optical aberrations of systems with annular pupils," *Appl. Opt.* **33**(34), 8125–8127 (1994).
24. V. N. Mahajan, *Optical Imaging and Aberrations Part I*, SPIE Press, Bellingham, Washington (1998).
25. J. Courtial and M. J. Padgett, "Performance of a cylindrical lens mode converter for producing Laguerre Gaussian laser modes," *Opt. Commun.* **159**(1–3), 13–18 (1999).
26. J. Carson et. al., "Direct imaging discovery of a 'Super-Jupiter' around the late B-type star κ And," *Astrophys. J. Lett.* **763**(2), L32 (2013).
27. A. M. Hughes et al., "Gas and dust emission at the outer edge of protoplanetary disks," *Astrophys. J.* **678**, 1119–1126 (2008).
28. K. Stapelfel, "Catalogue of circumstellar disks," (Oct. 2012), http://www.circumstellardisks.org/index.php (Jan. 2013).
29. J. T. Wright et al., "The exoplanet orbit database," *Astronom. Soc. Pacific* **123**(902), 412–422 (2011).
30. M. J. Ireland et al., "Two wide planetary-mass companions to solar-type stars in upper scorpius," *Astrophys. J.* **726**(2), 113 (2011).
31. H. B. Perets and M. B. N. Kouwenhoven, "On the origin of planets at very wide orbits from the recapture of free floating planets," *Astrophys. J.* **750**(1), 83 (2012).
32. F. Tamburini et al., "Overcoming the Rayleigh criterion limit with optical vortices," *Phys. Rev. Lett.* **97**(16), 163903 (2006).
33. S. Wolf et al."Circumstellar disks and planets," *Astron. Astrophys. Rev.* **20**, 52 (2012).

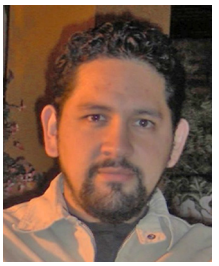

Juan P. Treviño is a PhD candidate at Instituto Nacional de Astrofísica, Optica y Electrónica. His main research interests are the mathematical modeling of light modal propagation and its applications to imaging systems such as the human eye and telescopes. He is also interested in the modeling and compensation of aberrations with adaptive optics systems for various applications.

Omar López-Cruz is a researcher at Instituto Nacional de Astrofísica, Optica y Electrónica, and visiting scientist at the Astrophyisics Group of the University of Bristol in the United Kingdom. His research interests range from stellar astrophysics, extragalactic astronomy, and observational cosmology. He uses all sorts of telescopes, interferometric arrays, and virtual observatories. He is leading a Mexican team of scientists and engineers to build a single-antenna experiment to search for the signs of the formation of the first stars in the universe using the 21 cm hyperfine transition of neutral hydrogen as a tracer.

Sabino Chávez-Cerda is a full-time researcher at Instituto Nacional de Astrofísica, Optica y Electrónica in the Optics department. He obtained his PhD degree from the Imperial College and has been recently appointed as fellow of the Optics Society of America. His main research fields are propagation of nondiffractive fields and rigorous mathematical physics aspects of optics.